

# Resonant emittance mixing of flat beams in plasma accelerators

S. Diederichs,<sup>1,2</sup> C. Benedetti,<sup>3</sup> A. Ferran Pousa,<sup>1</sup> A. Sinn,<sup>1</sup> J. Osterhoff,<sup>1,3</sup> C. B. Schroeder,<sup>3,4</sup> and M. Thévenet<sup>1,\*</sup>

<sup>1</sup>*Deutsches Elektronen-Synchrotron DESY, Notkestr. 85, 22607 Hamburg, Germany*

<sup>2</sup>*CERN, Espl. des Particules 1, 1211 Geneva, Switzerland*

<sup>3</sup>*Lawrence Berkeley National Laboratory, 1 Cyclotron Rd, Berkeley, California 94720, USA*

<sup>4</sup>*Department of Nuclear Engineering, University of California, Berkeley, California 94720, USA*

(Dated: March 12, 2024)

Plasma accelerators sustain large field gradients and could enable future compact linear colliders. To achieve the required high luminosity, linear colliders rely on flat beams to avoid potentially deleterious beamstrahlung effects. Here, we show that flat beams in plasma accelerators can be subject to beam quality degradation due to emittance mixing caused by transverse coupling in the wakefields. When there is a resonance between the betatron oscillations in the horizontal and vertical planes for the beam particles in a coupled wakefield, the transverse emittances fully exchange, leading to a round beam. Depending on the mechanism causing the resonance, the use of laser drivers, flat particle beam drivers, or hollow plasma channels can avoid the resonance and mitigate the emittance deterioration.

Plasma-based accelerators [1, 2] are promising prospects as drivers for future linear colliders due to their  $\gtrsim$  GV/m accelerating gradients. Although experimental progress in terms of energy gain [3–5], energy transfer efficiency [6], and energy spread preservation [7, 8] have increased the interest in plasma-based linear colliders [9–11], additional challenges must be overcome.

For optimal operation of a linear collider, the event rate and, consequently, the luminosity  $\mathcal{L}$  must be maximized while deleterious beamstrahlung effects [12] must be minimized. Because the former scales as  $\sim 1/(\sigma_x\sigma_y)$  [13] (where  $\sigma_x$  and  $\sigma_y$  are the rms beam sizes at the interaction point in the horizontal and vertical plane, respectively) and the latter as  $\sim 1/(\sigma_x + \sigma_y)$  [14], the solution adopted in the community is to operate with flat beams,  $\sigma_x \gg \sigma_y$ . This motivates the creation of beams with  $\epsilon_x/\epsilon_y \gg 1$  (where  $\epsilon_{[x,y]}$  is the beam emittance in  $[x, y]$ ), and the preservation of this ratio during acceleration. Known mechanisms that lead to deleterious exchange or mixing of the transverse emittances are linear coupling [15] due to misaligned or skew quadrupoles, and nonlinear coupling, e.g., due to space-charge effects [16, 17], which are mainly relevant at low energies. The later is known for the so-called Montague resonance that occurs if the focusing in the horizontal and vertical planes are in phase. In general, emittance mixing occurs when the equations of motion in  $x$  and  $y$  are coupled (for instance when the transverse force in  $x$  depends on  $y$ ) but such effects have not yet been described in plasma-based accelerators.

Plasma accelerators are often operated in the so-called blowout regime, where a particle beam or a laser driver is strong enough to expel all plasma electrons, creating a trailing ion cavity in its wake. In the ideal case of a uniform background ion distribution within the cavity, the transverse wakefields in  $x$  and  $y$  are decoupled, preventing emittance exchange. In practice, various nonlinear effects can perturb the transverse wakefields and cause

coupling, and, hence, emittance mixing. Such effects are almost inevitable for collider-relevant beams that require high charge ( $\sim$ nC) and low emittance ( $\sim$ 100 nm) and therefore generate extreme space-charge fields. In particular, such fields can further ionize the background plasma to higher levels [18] and/or cause ion motion [19], both of which can lead to the formation of nonlinearly coupled wakefields. Nonlinear wakefields are sometimes desired: for instance, nonlinearities in the wake due to, e.g., ion motion can suppress the hosing instability [20–22] while still allowing for witness beam emittance preservation through advanced matching schemes [23, 24].

In this Letter, we demonstrate by means of theory and 3D particle-in-cell (PIC) simulations that coupled wakefields in plasma accelerators can lead to severe emittance mixing of flat beams when there is a resonance between the betatron oscillations in the horizontal and vertical planes for the beam particles. With this effect, the horizontal emittance decreases as the vertical one increases, resulting in an overall growth of their geometric average. It is therefore different from the nonlinearity-induced mismatch, which causes emittance increase in both planes. While a radially symmetric nonlinear wakefield always results in full emittance exchange, breaking the radial symmetry (e.g., by using a flat driver causing ion motion) mitigates this effect by detuning the resonance. Emittance mixing must be taken into account when designing plasma-based colliders using flat beams. Although the acceleration of flat beams in nonlinear fields due to ion motion was previously considered [25], the coupling was overlooked because the modeled propagation distance was too short.

The effect of emittance mixing for flat beams in coupled, nonlinear wakefields is illustrated with a simple plasma-wakefield accelerator setup in the blowout regime that resembles the first stage of the proposed HALHF collider [9]. It consists of an electron drive beam, an electron witness beam, and a singly ionized lithium plasma

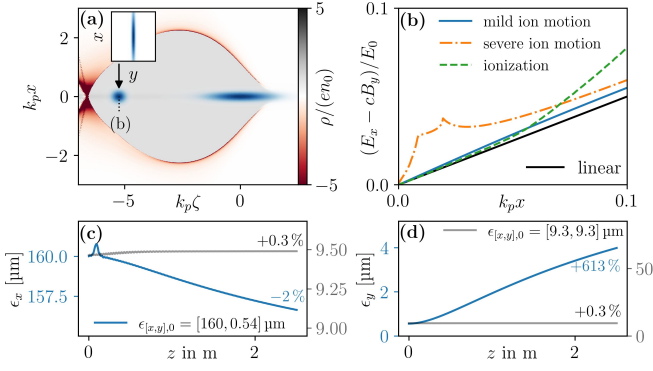


FIG. 1. (a) Normalized plasma charge density (grey-red color-scale) and drive and witness beams (blue) in the  $x$ - $\zeta$  plane, where  $\zeta = z - ct$  is the co-moving variable and  $c$  the speed of light; inset: transverse profile of the flat beam. (b) Examples of nonlinear transverse wakefields. The blue line (mild ion motion) corresponds to a lineout along the dashed line of the case in (a). Other colored lines correspond to wakefields obtained for severe ion motion (orange), induced by increasing the witness beam energy to 478 GeV, thereby decreasing the matched transverse spot size by  $\sim 10\times$ ; witness-beam-induced ionization (dashed green line), induced by replacing lithium with singly ionized argon. (c) and (d) Emittance in  $x$  and  $y$  planes, respectively, in the mild ion motion case for a flat beam (blue line) and a round beam (grey line) with the same initial  $\sqrt{\epsilon_x \epsilon_y}$ .

with a density of  $n_0 = 7 \times 10^{15} \text{ cm}^{-3}$ . The drive and witness beams have 4.3 nC and 1.6 nC of charge, respectively. The drive beam is bi-Gaussian with an emittance of  $\epsilon_{d,[x,y]} = 60 \mu\text{m}$ , rms length of  $\sigma_{d,z} = 42 \mu\text{m}$ , and is located at the origin. The witness beam is also bi-Gaussian with emittances of  $\epsilon_{w,x} = 160 \mu\text{m}$  and  $\epsilon_{w,y} = 0.54 \mu\text{m}$  in the horizontal and vertical plane, respectively. Its length is  $\sigma_{w,z} = 18 \mu\text{m}$  and it is located 334  $\mu\text{m}$  behind the drive beam. The drive and witness beams have initial energies of 31.9 GeV ( $\gamma_d = 62500$ ) and 5.1 GeV ( $\gamma_w = 10000$ ), and their transverse rms sizes are matched to the blowout wake. The simulations are conducted with the quasi-static, 3D PIC code HiPACE++ [26] using its mesh refinement capabilities. The complete numerical settings for all the simulations discussed in this paper available online [27]. In what follows,  $E_0 = m_e c^2 k_p / e$  is the cold, non-relativistic wavebreaking limit,  $k_p = \omega_p / c$  the plasma wavenumber,  $\omega_p = \sqrt{n_0 e^2 / (m_e \epsilon_0)}$  the plasma frequency, and  $\epsilon_0$  the vacuum permittivity.

The wake and nonlinear wakefields causing coupling are shown in Fig. 1. The resulting emittance exchange can be seen in Fig. 1 (c) and (d) as the witness beam is accelerated from 5.1 to  $\sim 21$  GeV. For a flat witness beam, the (large) horizontal emittance decreases by 3.4  $\mu\text{m}$ , or 2%. At the same time, the (small) vertical emittance increases by 3.4  $\mu\text{m}$ , or 613%. As the luminosity scales as the inverse of the geometric average of the emittances in  $x$  and  $y$ , i.e. as  $\sqrt{\epsilon_x \epsilon_y}$ , this quantity is tracked in the

rest of this work. In the example of Fig. 1, it increases by a factor of 2.6, so the luminosity is decreased by this factor. Notably, a round beam with the same initial  $\sqrt{\epsilon_x \epsilon_y}$  sees only a small growth of 0.3%, showing that the drive-beam-induced nonlinearity of the transverse field is not a problem *per se*.

The behavior of the emittance mixing is investigated by tracking test particles in an analytic, coupled wakefield using the tracking code Wake-T [28]. In the case of a high-density particle beam, which perturbs the ion background and leads to nonlinear fields, the perturbed wakefields can be described analytically in the nonrelativistic ion motion regime in certain cases [23]. Here, a simplified, approximate model for the perturbed transverse wakefields is used with  $W_x = E_x - cB_y = (k_p x E_0 / 2) \{1 + \alpha_x H[r^2 / (2L_x^2)]\}$  and  $W_y = E_y + cB_x = (k_p y E_0 / 2) \{1 + \alpha_y H[r^2 / (2L_y^2)]\}$ , where  $H(q) = [1 - \exp(-q)]/q$ ,  $r = (x^2 + y^2)^{1/2}$  is the radius, and  $L_{[x,y]}$  and  $\alpha_{[x,y]}$  the characteristic size and amplitude of the nonlinearity, respectively. The coupling comes from the  $r$ -dependency of the nonlinear term.

Test particle beams with the same parameters as the flat witness beam in Fig. 1 are propagated for 10 m, neglecting acceleration, in analytic wakefields with different values of  $\alpha_{[x,y]}$  and  $L_{[x,y]}$ . We consider two cases that approximately describe the regimes of ① ion motion induced by an axisymmetric drive beam ( $\alpha_{[x,y]} = 1$  and  $L_{[x,y]} = \sigma_{d,[x,y]} = 6 \mu\text{m}$ ), and ② ion motion induced by a flat witness beam ( $\alpha_x = 0.5$  and  $L_y = 0.5L_x$ ,  $\alpha_y$  and  $L_x$  as in ①). For case ②, the nonlinearity is stronger along the  $y$ -axis and the length scale is shorter. The resulting growth of  $\sqrt{\epsilon_x \epsilon_y}$  for these cases is 8.5x and 7.1x, respectively, and the axisymmetric case ① results in a round beam. The mixing can be observed in the final distributions shown in Fig. 2.

These two cases result in different characteristic particle trajectories, as shown on the right of Fig. 2. For the axisymmetric nonlinearity of ①, the particle's elliptical orbit in the  $x$ - $y$  plane precesses at a constant frequency. This precession frequency depends on the particle's initial conditions, so the beam relaxes to a round beam with full emittance mixing. For a non-axisymmetric nonlinearity such as in ②, the precession frequency varies along the trajectory, and one typical behavior is shown on Fig. 2, where the major axis of the ellipse performs full rotations in the  $x$ - $y$  plane. The other typical behavior for case ② (not shown here) consists of a *bound* trajectory: the major axis oscillates around the  $x$  axis, so the amplitude of betatron oscillations in  $y$  remains small. This limits the emittance growth and prevents the equalization of  $\epsilon_x$  and  $\epsilon_y$ .

The qualitative behaviors do not depend on the specific profile of the nonlinearity, and can be captured by a reduced model in the analytic fields of a quadratic nonlinearity (only used in this paragraph)  $W_x = k_p x E_0 (1/2 +$

$r^2/\ell_x^2$ ) and  $W_y = k_p y E_0 (1/2 + r^2/\ell_y^2)$ , where  $\ell_x$  and  $\ell_y$  are the length scales of the nonlinearity in the  $x$  and  $y$  directions, respectively. The resulting equations of motion are similar to Eqs. (9) and (10) of Ref. [29], and the slowly varying component of the transverse dynamics can be derived following the same approach and assuming  $k_p \ell_{[x,y]} \ll 1$  (see Supplemental Material for details). For the axisymmetric case ① where  $\ell_x = \ell_y = \ell$ , and for the *bound* behavior of case ②, the direction of the major axis of the particle's ellipse in the  $x$ - $y$  plane is periodic and the periods read, respectively,

$$\omega_p T_{sym} = \frac{2\pi\gamma k_p \ell^2}{|x_0 u_{y0}|}, \quad \omega_p T_{asym} = \frac{16\pi}{\sqrt{6}} \frac{\sqrt{\gamma} \ell_y^2}{x_0^2}, \quad (1)$$

for an electron starting on the  $x$  axis at  $x_0$ , with transverse momentum only in the  $y$  direction  $u_{y0}$  and Lorentz factor  $\gamma$ . A comparison between these expressions and the numerical integration of the equation of motion in the presence of the quadratic nonlinearity are shown on Fig. 2 (b). An excellent agreement is observed, even for the strongest nonlinearity ( $k_p \ell_y < 1$ ).

The impact of the coupled nonlinearity of the wakefields on the final emittance is further investigated with a 2D parameter scan. The scan is spanning  $\alpha_{[x,y]} = [0.0, 0.0] \times [2.5, 2.5]$  with 5200 Wake-T simulations using Optimas [30], an open-source Python library to run ensembles of numerical simulations and optimization tasks. The beam is propagated over 100 m to ensure saturation of the emittance. The final growth of  $\sqrt{\epsilon_x \epsilon_y}$  in percent for working point ① ( $L_x = L_y$ ) is shown in Fig. 2 (c). For  $\alpha_y = \alpha_x$  (resonant) the emittance mixing is maximal, resulting in a round beam. For  $\alpha_y > \alpha_x$  (stronger nonlinearity in the small axis of the flat beam), the emittance growth falls off quickly and is dominated by the mismatch of the nonlinear fields since the emittance in  $x$  (not shown) does not decrease in this regime. For  $\alpha_y < \alpha_x$ , the emittance growth due to mixing decreases and eventually vanishes.

Notably, the final emittance only depends on the angle  $\arctan(\alpha_y/\alpha_x)$ , as can be seen on Fig. 2 (d), where the blue line uses the same data as Fig. 2 (c). Working point ① is taken on-resonance from this scan. When the nonlinearity length scale is different in  $x$  and  $y$ , the resonance occurs at a different angle, as can be seen on the orange curve of Fig. 2 (d), where  $L_y = 0.5L_x$ . Working point ② is taken off-resonance from this scan. In both cases, the resonance results in full mixing and maximum growth of  $\sqrt{\epsilon_x \epsilon_y}$ .

The emittance mixing in a flat witness beam can be understood in terms of resonance of betatron oscillations in the horizontal and vertical planes for the beam particles when a nonlinearity in the wakefield couples the motion in these planes. Particles for which the horizontal and vertical betatron frequencies are almost equal are called resonant. For these particles, the coupling of the

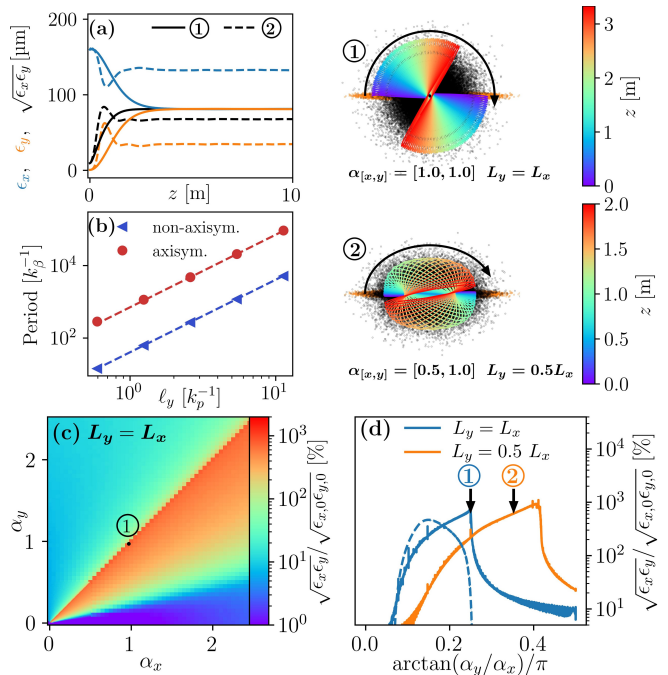


FIG. 2. (a) Evolution of emittances  $\epsilon_x$  (blue),  $\epsilon_y$  (orange), and  $\sqrt{\epsilon_x \epsilon_y}$  (black) vs. propagation distance of a flat beam for the two working points ① and ② shown in (d). Their corresponding initial (orange) and final (black)  $x$ - $y$  phase space are shown on the right. The colored lines in the insets denote the trajectory of a single particle. (b) Precession period for working points ① (resonant) and ② (detuned), comparing theory (dashed line) and particle tracking (markers). (c) Final  $\sqrt{\epsilon_x \epsilon_y}$  at saturation as a function of  $\alpha_x$  and  $\alpha_y$  for  $L_y = L_x$ . (d)  $\sqrt{\epsilon_x \epsilon_y}$  at saturation as a function of the angle  $\arctan(\alpha_y/\alpha_x)/\pi$  for  $L_y = L_x$  and  $L_y = 0.5L_x$  for particle tracking (solid lines) and theory (dashed line).

wakefields causes a decay in betatron amplitude in the  $x$  plane and a growth in the  $y$  plane. This results in the decrease of the horizontal beam emittance and the increase of the vertical one. A simplified model predicting the emittance growth by determining the fraction of beam particles that are resonant can be found in the Supplemental Material. The growth of  $\sqrt{\epsilon_x \epsilon_y}$  obtained from the model for the case  $L_x = L_y$  is shown in Fig. 2 (d), showing good agreement with test particles. The emittance growth for angles  $> 0.25\pi$  in the particle tracking simulations are caused by nonlinearity-induced mismatch, which is not included in the model. Figures 2 (c) and (d) show promising regions for  $\alpha_{[x,y]}$  where the growth of  $\sqrt{\epsilon_x \epsilon_y}$  is minimal. However, it is not clear whether these regions can be attained in a realistic plasma accelerator where the strength of the nonlinearity  $\alpha_{[x,y]}$  and length scales  $L_{[x,y]}$  may not be chosen independently as they depend on the full beam distribution.

To capture the full dynamics of emittance mixing under realistic conditions, including, in particular, ion motion effects caused by the witness beam and its feed-

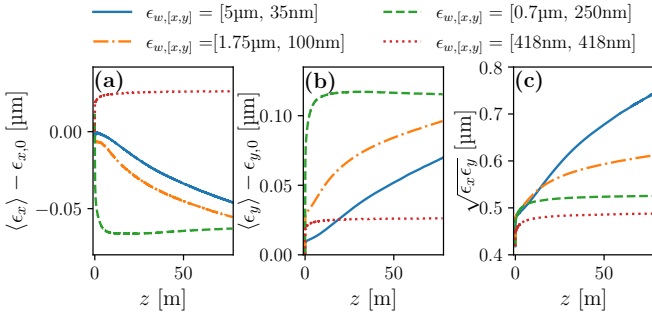


FIG. 3. Evolution of emittances (a)  $\epsilon_x$ , (b)  $\epsilon_y$ , and (c)  $\sqrt{\epsilon_x \epsilon_y}$ , with different initial values for the horizontal and vertical emittances for the witness bunch, but the same initial  $\sqrt{\epsilon_x \epsilon_y}$ . The average slice emittance (subtracted by the initial emittance) is used in (a) and (b) to avoid head-to-tail mismatches that lead to an increase in the emittance in  $x$  and mask the mixing, while (c) shows the projected emittance.

back on the beam propagation, we hereafter turn to HiPACE++ simulations. We choose parameters in the witness beam-induced ion motion regime. The same parameters as in Fig. 1 are used, except for the witness beam emittance of  $\epsilon_{w,[x,y]} = [5 \mu\text{m}, 35 \text{nm}]$ , which corresponds to the proposed emittance of the International Linear Collider (ILC) [31]. At a plasma density of  $n_0 = 7 \times 10^{15} \text{cm}^{-3}$ , the space charge fields of the matched beam at  $\gamma_w = 10000$  exceeds 300 GV/m. To preclude ionization effects of the background ions, fully ionized hydrogen is used, although another sufficiently ionized element could work. To further mitigate ion motion from the drive beam, a large emittance of  $\epsilon_{d,[x,y]} = 2.8 \text{mm}$  is used and the drive beam is made rigid to preclude any effects caused by its evolution. The witness beam is propagated over a distance of 77.5 m and gains energy from 5.1 to 500 GeV.

Figure 3 shows the emittance evolution from 4 different witness beams with decreasing flatness (from very flat to round with the same initial  $\sqrt{\epsilon_x \epsilon_y}$ ):  $\epsilon_{w,x} = 5 \mu\text{m}$ ,  $1.75 \mu\text{m}$ ,  $0.7 \mu\text{m}$  and  $418 \text{nm}$  while  $\epsilon_{w,y} = 35 \text{nm}$ ,  $100 \text{nm}$ ,  $250 \text{nm}$  and  $418 \text{nm}$ , respectively. In all flat beam cases, the emittance in  $x$  decreases while it increases in  $y$ . A flatter beam results in a slower growth of  $\sqrt{\epsilon_x \epsilon_y}$  to a larger saturated value, such that the flattest beams do not reach saturation after acceleration to 500 GeV. Therefore, for ILC-like beams with  $\epsilon_{w,[x,y]} = [5 \mu\text{m}, 35 \text{nm}]$ , this effect needs to be assessed in the context of using them for a multi-TeV-class plasma-based collider [10]. The emittance of the round beam increases in both planes by 6% due to the nonlinearity of the ion-motion-perturbed fields, which can be avoided by perfectly matching the beam to the nonlinear fields [23, 24]. The emittances of the flat beams increase by 26%, 46%, and 78%, respectively.

In what follows, we assess the emittance mixing in the HALHF collider proposal with additional sources of

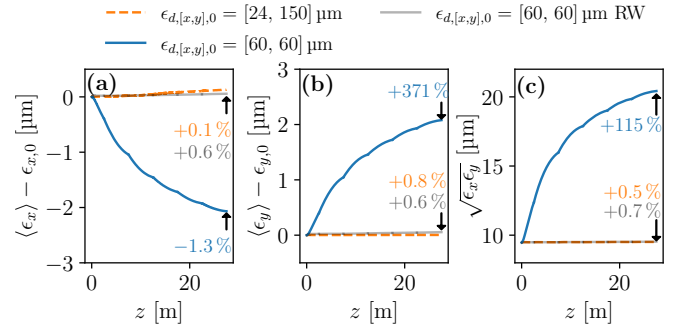


FIG. 4. Evolution of emittances (a)  $\epsilon_x$ , (b)  $\epsilon_y$ , and (c)  $\sqrt{\epsilon_x \epsilon_y}$ , for a flat witness beam and a round driver (blue lines), a flat witness beam and a flat driver (orange lines), and a round witness and a round driver (grey lines). As in Fig. 3, (a) and (b) show average slice emittance and (c) shows the projected emittance.

nonlinearity, and propose a mitigation method using a flat driver. The HALHF collider is proposed to consist of 16 stages, with the first stage being 2.5 m, and the other stages being each 5 m long. The emittance of the drive beam has a strong impact on the design: while a larger emittance increases the deleterious effect of head erosion [32], a small emittance increases driver-induced ion motion, a modest amount of which can result in significant emittance mixing as shown in Fig. 1. An emittance of  $\epsilon_{d,[x,y]} = 60 \mu\text{m}$  was found to be a reasonable trade-off. Sodium was chosen instead of argon as background plasma source, since the second ionization level is at 47 eV instead of 27 eV, preventing additional detrimental ionization in the first stages.

The first 6 stages of the HALHF collider are simulated in a simplified way: the transport between stages is neglected, i.e., the witness beam is transferred to the next stage without further modifications while the drive beam is replenished. The evolution of emittances of the flat witness beam is shown in Fig. 4. A round drive beam with  $\epsilon_{d,[x,y]} = 60 \mu\text{m}$  shows large emittance mixing in the witness beam: the averaged slice emittance in the vertical plane increases by 371%, and  $\sqrt{\epsilon_x \epsilon_y}$  by 115%. The emittance of a round witness beam with the same initial  $\sqrt{\epsilon_x \epsilon_y}$  increases by less than 1% [33]. The dramatic emittance growth for the flat witness beam is caused by the mild but symmetric ion motion induced by the drive beam, resulting in resonant mixing. Avoiding the resonance efficiently mitigates this effect: using a flat drive beam with emittances  $\epsilon_{d,[x,y]} = [24 \mu\text{m}, 150 \mu\text{m}]$  causes asymmetric ion motion and suppresses emittance mixing. The quantity  $\sqrt{\epsilon_x \epsilon_y}$  increases by less than 1% in the flat drive beam case.

In this Letter we have shown that nonlinear transverse wakefields in plasma accelerators couple the motion in the transverse planes and can severely affect the beam quality of flat witness beams through emittance mixing. This emittance mixing relies on a resonance between the

betatron oscillations in the horizontal and vertical planes, and if the nonlinearity is axisymmetric, an initially flat beam becomes round after mixing. Breaking the resonance effectively mitigates the beam degradation, which can be achieved, for instance, with flat drive beams (so the nonlinear focusing force is not axisymmetric) or using a laser driver (for which ion motion is negligible).

Nonlinearities due to ionization or ion motion by the witness beam itself are almost inevitable for collider-relevant beam parameters (high charge, high energy, low emittance) in a uniform plasma. Therefore, emittance mixing must be considered and suppressed when designing plasma-based colliders with flat witness beams in the plasma accelerators. The choice of the element used to generate the plasma is decisive: emittance mixing can be controlled by avoiding both ion motion (stronger for elements with larger charge-to-mass ratio, i.e., light elements or heavy elements ionized to high levels) and beam-induced ionization (stronger for heavy elements when not sufficiently ionized).

While only the blowout regime was discussed in details, emittance mixing can also occur in other regimes such as the linear and quasi-linear regimes [34] as well as plasma-based positron acceleration schemes [35–38] that operate with coupled, nonlinear focusing fields. Emittance mixing in plasma accelerators can be fully circumvented by using hollow core plasma channels [39] or by accelerating round beams [11].

We acknowledge fruitful discussions with Reinhard Brinkmann, Carl A. Lindstrøm, Ming Zeng, and Eric Esarey. We acknowledge the Funding by the Helmholtz Matter and Technologies Accelerator Research and Development Program. This work was supported by the Director, Office of Science, Office of High Energy Physics, of the U.S. Department of Energy, under Contract No. DE-AC02-05CH11231, and used the computational facilities at the National Energy Research Scientific Computing Center (NERSC). We gratefully acknowledge the Gauss Centre for Supercomputing e.V. ([www.gauss-centre.eu](http://www.gauss-centre.eu)) for funding this project by providing computing time through the John von Neumann Institute for Computing (NIC) on the GCS Supercomputer JUWELS at Jülich Supercomputing Centre (JSC). This research was supported in part through the Maxwell computational resources operated at Deutsches Elektronen-Synchrotron DESY, Hamburg, Germany.

The input scripts for all simulations used in this Letter are available online [27].

---

\* maxence.thevenet@desy.de

[1] T. Tajima and J. M. Dawson, *Phys. Rev. Lett.* **43**, 267 (1979).  
 [2] P. Chen, J. M. Dawson, R. W. Huff, and T. Katsouleas, *Phys. Rev. Lett.* **54**, 693 (1985).

[3] I. Blumenfeld, C. E. Clayton, F.-J. Decker, M. J. Hogan, C. Huang, R. Ischebeck, R. Iverson, C. Joshi, T. Katsouleas, N. Kirby, W. Lu, K. A. Marsh, W. B. Mori, P. Muggli, E. Oz, R. H. Siemann, D. Walz, and M. Zhou, *Nature* **445**, 741 (2007).  
 [4] A. Gonsalves, K. Nakamura, J. Daniels, C. Benedetti, C. Pieronek, T. de Raadt, S. Steinke, J. Bin, S. Bulanov, J. van Tilborg, *et al.*, *Physical Review Letters* **122**, 084801 (2019).  
 [5] C. Aniculaesei, T. Ha, S. Yoffe, L. Labun, S. Milton, E. McCary, M. M. Spinks, H. J. Quevedo, O. Z. Labun, R. Sain, A. Hannasch, R. Zgadzaj, I. Pagano, J. A. Franco-Altamirano, M. L. Ringuette, E. Gaul, S. V. Luedtke, G. Tiwari, B. Ersfeld, E. Brunetti, H. Ruhl, T. Ditmire, S. Bruce, M. E. Donovan, M. C. Downer, D. A. Jaroszynski, and B. M. Hegelich, *Matter and Radiation at Extremes* **9**, 014001 (2023).  
 [6] M. Litos, E. Adli, W. An, C. I. Clarke, C. E. Clayton, S. Corde, J. P. Delahaye, R. J. England, A. S. Fisher, J. Frederico, S. Gessner, S. Z. Green, M. J. Hogan, C. Joshi, W. Lu, K. A. Marsh, W. B. Mori, P. Muggli, N. Vafaei-Najafabadi, D. Walz, G. White, Z. Wu, V. Yakimenko, and G. Yocky, *Nature* **515**, 92 (2014).  
 [7] M. Kirchen, S. Jalas, P. Messner, P. Winkler, T. Eichner, L. Hübner, T. Hülsenbusch, L. Jeppe, T. Parikh, M. Schnepp, and A. R. Maier, *Phys. Rev. Lett.* **126**, 174801 (2021).  
 [8] C. A. Lindstrøm, J. M. Garland, S. Schröder, L. Boulton, G. Boyle, J. Chappell, R. D’Arcy, P. Gonzalez, A. Knetch, V. Libov, G. Loisch, A. Martinez de la Ossa, P. Niknejadi, K. Pöder, L. Schaper, B. Schmidt, B. Sheeran, S. Wesch, J. Wood, and J. Osterhoff, *Phys. Rev. Lett.* **126**, 014801 (2021).  
 [9] B. Foster, R. D’Arcy, and C. A. Lindstrøm, *New Journal of Physics* **25**, 093037 (2023).  
 [10] E. Adli, J.-P. Delahaye, S. J. Gessner, M. J. Hogan, T. Raubenheimer, W. An, C. Joshi, and W. Mori, in *Proceedings, Community Summer Study 2013: Snowmass on the Mississippi (CSS2013): Minneapolis, MN, USA, July 29-August 6, 2013* (2013) arXiv:1308.1145 [physics.acc-ph].  
 [11] C. Schroeder, F. Albert, C. Benedetti, J. Bromage, D. Bruhwiler, S. Bulanov, E. Campbell, N. Cook, B. Cros, M. Downer, E. Esarey, D. Froula, M. Fuchs, C. Geddes, S. Gessner, A. Gonsalves, M. Hogan, S. Hooker, A. Huebl, C. Jing, C. Joshi, K. Krushelnick, W. Leemans, R. Lehe, A. Maier, H. Milchberg, W. Mori, K. Nakamura, J. Osterhoff, J. Palastro, M. Palmer, K. Pöder, J. Power, B. Shadwick, D. Terzani, M. Thévenet, A. Thomas, J. van Tilborg, M. Turner, N. Vafaei-Najafabadi, J.-L. Vay, T. Zhou, and J. Zuegel, *Journal of Instrumentation* **18**, T06001 (2023).  
 [12] J. E. Augustin, N. Dikansky, Y. Derbenev, J. Rees, B. Richter, A. Skrinsky, M. Tigner, and H. Wiedemann, *eConf* **C781015**, 009 (1978).  
 [13] D. Schulte, *Reviews of Accelerator Science and Technology* **09**, 209 (2016).  
 [14] C. Schroeder, C. Benedetti, S. Bulanov, D. Terzani, E. Esarey, and C. Geddes, *Journal of Instrumentation* **17**, P05011 (2022).  
 [15] D. A. Edwards and M. J. Syphers, *An Introduction to the Physics of High Energy Accelerators*, Wiley Series in Beam Physics and Accelerator Technology (Wiley, 2008).  
 [16] B. Montague, “Fourth-order coupling resonance excited

- by space charge forces in a synchrotron,” (1968).
- [17] I. Hofmann, *Space charge physics for particle accelerators* (Springer, 2017).
  - [18] D. L. Bruhwiler, D. Dimitrov, J. R. Cary, E. Esarey, W. Leemans, and R. E. Giacone, *Physics of Plasmas* **10**, 2022 (2003).
  - [19] J. B. Rosenzweig, A. M. Cook, A. Scott, M. C. Thompson, and R. B. Yoder, *Phys. Rev. Lett.* **95**, 195002 (2005).
  - [20] T. J. Mehrling, C. Benedetti, C. B. Schroeder, E. Esarey, and W. P. Leemans, *Phys. Rev. Lett.* **121**, 264802 (2018).
  - [21] S. Diederichs, C. Benedetti, M. Thévenet, E. Esarey, J. Osterhoff, and C. B. Schroeder, *Phys. Rev. Accel. Beams* **25**, 091304 (2022).
  - [22] S. Diederichs, C. Benedetti, E. Esarey, M. Thévenet, J. Osterhoff, and C. B. Schroeder, *Physics of Plasmas* **29**, 043101 (2022).
  - [23] C. Benedetti, C. B. Schroeder, E. Esarey, and W. P. Leemans, *Phys. Rev. Accel. Beams* **20**, 111301 (2017).
  - [24] C. Benedetti, T. J. Mehrling, C. B. Schroeder, C. G. R. Geddes, and E. Esarey, *Physics of Plasmas* **28**, 053102 (2021), <https://doi.org/10.1063/5.0043847>.
  - [25] W. An, W. Lu, C. Huang, X. Xu, M. J. Hogan, C. Joshi, and W. B. Mori, *Phys. Rev. Lett.* **118**, 244801 (2017).
  - [26] S. Diederichs, C. Benedetti, A. Huebl, R. Lehe, A. Myers, A. Sinn, J.-L. Vay, W. Zhang, and M. Thévenet, *Computer Physics Communications* **278**, 108421 (2022).
  - [27] S. Diederichs, C. Benedetti, A. Ferran Pousa, A. Sinn, J. Osterhoff, C. B. Schroeder, and M. Thévenet, “Input scripts for ”Emittance mixing of flat beams in plasma accelerators”,” (2024).
  - [28] A. Ferran Pousa, R. Assmann, and A. Martinez de la Ossa, *Journal of Physics: Conference Series* **1350**, 012056 (2019).
  - [29] Y. Liu and M. Zeng, *Physical Review Accelerators and Beams* **26**, 031301 (2023).
  - [30] A. Ferran Pousa, S. Jalas, M. Kirchen, A. Martinez de la Ossa, M. Thévenet, S. Hudson, J. Larson, A. Huebl, J.-L. Vay, and R. Lehe, *Phys. Rev. Accel. Beams* **26**, 084601 (2023).
  - [31] A. Aryshev, et al., “The international linear collider: Report to snowmass 2021,” (2022).
  - [32] W. An, M. Zhou, N. Vafaei-Najafabadi, K. A. Marsh, C. E. Clayton, C. Joshi, W. B. Mori, W. Lu, E. Adli, S. Corde, M. Litos, S. Li, S. Gessner, J. Frederico, M. J. Hogan, D. Walz, J. England, J. P. Delahaye, and P. Muggli, *Phys. Rev. ST Accel. Beams* **16**, 101301 (2013).
  - [33] Singly ionized lithium was used here, since the space charge fields of the round witness beam were strong enough to ionize sodium. Note that the lighter lithium enables more ion motion.
  - [34] E. Esarey, C. B. Schroeder, and W. P. Leemans, *Rev. Mod. Phys.* **81**, 1229 (2009).
  - [35] S. Zhou, J. Hua, W. An, W. B. Mori, C. Joshi, J. Gao, and W. Lu, *Phys. Rev. Lett.* **127**, 174801 (2021).
  - [36] K. V. Lotov, *Physics of Plasmas* **14**, 023101 (2007).
  - [37] T. Silva, L. D. Amorim, M. C. Downer, M. J. Hogan, V. Yakimenko, R. Zgadzaj, and J. Vieira, *Phys. Rev. Lett.* **127**, 104801 (2021).
  - [38] S. Diederichs, T. J. Mehrling, C. Benedetti, C. B. Schroeder, A. Knetsch, E. Esarey, and J. Osterhoff, *Phys. Rev. Accel. Beams* **22**, 081301 (2019).
  - [39] C. Schroeder, C. Benedetti, E. Esarey, and W. Leemans, *Nuclear Instruments and Methods in Physics Research*

Section A: Accelerators, Spectrometers, Detectors and Associated Equipment **829**, 113 (2016).

# Supplemental Material: Resonant emittance mixing of flat beams in plasma accelerators

## I. ANALYTICAL MODEL FOR PRECESSION DYNAMICS

We consider a simplified profile for the nonlinearity with transverse wakefields given by

$$\begin{aligned} W_x &= k_p x E_0 \left( \frac{1}{2} + \frac{r^2}{\ell_x^2} \right) \\ W_y &= k_p y E_0 \left( \frac{1}{2} + \frac{r^2}{\ell_y^2} \right) \end{aligned} \quad (\text{S1})$$

where  $\ell_x$  and  $\ell_y$  are the length scales of the nonlinearity in the  $x$  and  $y$  directions, respectively. Acceleration is neglected. The resulting equation of motion is similar to Eqs. (9)–(10) of Ref. [29], where only the last term is conserved, and the slowly-varying component of the transverse dynamics can be derived following the same approach and assuming  $k_p \ell_{[x,y]} \ll 1$ . Introducing complex variables [see Eqs. (12-13) of Ref. [29]]

$$\begin{aligned} U &= (k_p x - i\sqrt{2\gamma\beta_x}) \exp(-i\omega_\beta t) \\ V &= (k_p y - i\sqrt{2\gamma\beta_y}) \exp(-i\omega_\beta t) \end{aligned} \quad (\text{S2})$$

where  $i$  is the imaginary number,  $\beta_x$  is the transverse velocity normalized to the speed of light and  $\omega_\beta = \omega_p/\sqrt{2\gamma}$  is the betatron frequency, the transverse equations of motion averaged over one betatron period become [to be compared with Eq. (16) of Ref. [29]]

$$\begin{aligned} \frac{dU}{\omega_\beta dt} &= \sqrt{\frac{2}{\gamma}} \frac{i}{8(k_p \ell_x)^2} (3|U|^2 U + V^2 U^* + 2|V|^2 U) \\ \frac{dV}{\omega_\beta dt} &= \sqrt{\frac{2}{\gamma}} \frac{i}{8(k_p \ell_y)^2} (3|V|^2 V + U^2 V^* + 2|U|^2 V). \end{aligned} \quad (\text{S3})$$

Using the polar representation for  $U = |U| \exp(i\Phi_x)$  and  $V = |V| \exp(i\Phi_y)$ , one gets the following equations of motion:

$$\begin{aligned} \frac{d|U|^2}{\omega_\beta dt} &= -\sqrt{\frac{2}{\gamma}} \frac{1}{4(k_p \ell_x)^2} |U|^2 |V|^2 \sin 2\Delta\Phi \\ \frac{d|V|^2}{\omega_\beta dt} &= +\sqrt{\frac{2}{\gamma}} \frac{1}{4(k_p \ell_y)^2} |U|^2 |V|^2 \sin 2\Delta\Phi \\ \frac{d\Phi_x}{\omega_\beta dt} &= \sqrt{\frac{2}{\gamma}} \frac{1}{8(k_p \ell_x)^2} (3|U|^2 + 2|V|^2 + |V|^2 \cos 2\Delta\Phi) \\ \frac{d\Phi_y}{\omega_\beta dt} &= \sqrt{\frac{2}{\gamma}} \frac{1}{8(k_p \ell_y)^2} (3|V|^2 + 2|U|^2 + |U|^2 \cos 2\Delta\Phi) \end{aligned} \quad (\text{S4})$$

where  $\Delta\Phi = \Phi_y - \Phi_x$ . Note the similarity with Eq. (S24), obtained with a slightly different approach but similar approximations. This system of equations can be solved

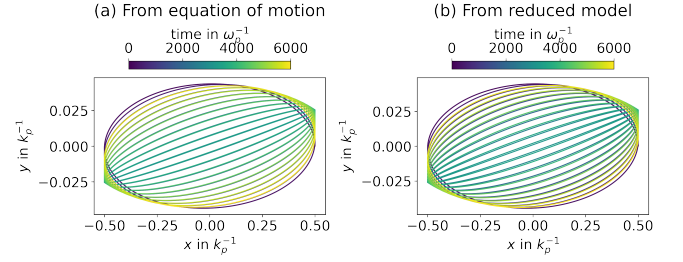


FIG. S1. (a) Trajectory of a test particle in forces given by Eqs. (S1), by numerical integration of the equations of motion directly. (b) same as (a) solving for the reduced model of Eqs. (S4). Here,  $\ell_x^2 = \infty$ ,  $\ell_y^2 = 5$  and the particle starts with  $x_0 = 0.5$ ,  $y_0 = 0$ ,  $p_{x,0} = 0$ , and  $p_{y,0} = 1$ .

numerically for  $|U|$ ,  $|V|$ ,  $\Phi_x$  and  $\Phi_y$ , and the  $x$  and  $y$  positions can be reconstructed using (S2). The comparison is shown on Fig. S1, demonstrating excellent agreement with directly solving for the equations of motion numerically. The precession behavior is properly captured by the reduced model. As done in Ref. [29], the slowly varying properties of the electron's orbit can be obtained with initial conditions  $y_0 = 0$  and  $p_{x,0} = 0$ .

When the nonlinearity is axisymmetric ( $\ell_x = \ell_y$ ), the particle traces an ellipse in the  $x$ - $y$  space with constant precession rate. The precession period  $T_{prec}$  is obtained with the similar approach as Eq. (37) of Ref. [29], and reads

$$\omega_p T_{sym} = \frac{2\pi\gamma k_p \ell^2}{|x_0 u_{y0}|} \quad (\text{S5})$$

where  $\ell = \ell_x = \ell_y$ .

When the nonlinearity is not axisymmetric, in particular assuming  $\ell_x \rightarrow \infty$ , the major axis of the ellipse oscillates around the  $x$  axis (such that the precession rate is not constant). The period of these oscillations can be calculated by further assuming that the amplitudes of betatron oscillations in both directions  $|U|^2$  and  $|V|^2$  are constant with  $|V|^2 \ll |U|^2$ . Equations (S4) can then be simplified, yielding in particular  $\Phi_x = const$ , and  $\Phi_y$  can be integrated analytically to give the following period of oscillations:

$$\omega_p T_{asym} = \frac{16\pi}{\sqrt{6}} \frac{\sqrt{\gamma} \ell_y^2}{x_0^2}. \quad (\text{S6})$$

## II. ANALYTICAL MODEL FOR EMITTANCE MIXING IN FLAT BEAMS

The emittance mixing in a flat witness beam can be understood in terms of resonance of betatron oscillations in the horizontal and vertical planes for the beam particles when a nonlinearity in the wakefield couples the motion in these planes.

We consider the following transverse equations of motion for the witness beam particles (written in a compact form),

$$\begin{cases} \frac{d[x,y]}{dz} = \frac{u_{[x,y]}}{\gamma_w} \\ \frac{du_{[x,y]}}{dz} = -\frac{k_p^2[x,y]}{2} \left[ 1 + \alpha_{[x,y]} H\left(\frac{r^2}{2L_{[x,y]}^2}\right) \right], \end{cases} \quad (\text{S7})$$

where  $z$  is the propagation distance ( $z = ct$ , with  $t$  the time, since we consider relativistic particles),  $x$  ( $y$ ) is the transverse coordinates of the particle in the horizontal (vertical) plane,  $u_x$  ( $u_y$ ) the horizontal (vertical) component of the transverse momentum (normalized to  $m_e c$ ),  $r^2 = x^2 + y^2$ ,  $H(q) = [1 - \exp(-q)]/q$ ,  $\gamma_w \gg 1$  the relativistic factor for the particle,  $\alpha_{[x,y]}$  the nonlinearity coefficients, and  $L_{[x,y]}$  the characteristic sizes of the nonlinearity.

We introduce action-angle coordinates, defined as

$$\begin{cases} [x,y] = \left(\frac{2j_{[x,y]}}{\gamma_w k_{\beta,0}}\right)^{1/2} \cos \theta_{[x,y]} \\ u_x = -\left(2\gamma_w k_{\beta,0} j_{[x,y]}\right)^{1/2} \sin \theta_{[x,y]}, \end{cases} \quad (\text{S8})$$

where  $j_x$  ( $j_y$ ) and  $\theta_x$  ( $\theta_y$ ) are, respectively, the action and angle coordinates in the horizontal (vertical) plane, and  $k_{\beta,0} = k_p/(2\gamma_w)^{1/2}$  is the linear (i.e., unperturbed) betatron wavenumber. Motion of beam particles is easier to analyze using these coordinates, as opposed to Cartesian coordinates, since the symmetries of the problem (e.g., quasi-periodic motion) become explicit.

Rewriting the equations of motion Eq. (S7) using action-angle coordinates we obtain

$$\begin{cases} \frac{d\theta_{[x,y]}}{dz} = k_{\beta,0} \left[ 1 + \alpha_{[x,y]} \cos^2 \theta_{[x,y]} H\left(\frac{r^2}{2L_{[x,y]}^2}\right) \right] \\ \frac{dj_{[x,y]}}{dz} = \alpha_{[x,y]} k_{\beta,0} j_{[x,y]} \sin 2\theta_{[x,y]} H\left(\frac{r^2}{2L_{[x,y]}^2}\right), \end{cases} \quad (\text{S9})$$

where  $r^2 = 2(j_x \cos^2 \theta_x + j_y \cos^2 \theta_y)/\gamma_w k_{\beta,0}$ . We see that the system can be described as a set of nonlinearly-coupled oscillators.

For the beam initial condition considered in this work (i.e., a Gaussian beam distribution linearly matched in the unperturbed wakefield with  $\epsilon_{w,[x,y]}$  the rms emittances on each plane) the initial angles,  $\theta_{[x,y],0}$ , are uniformly distributed in  $[0, 2\pi]$ , and the initial actions,  $j_{[x,y],0}$ , are distributed as

$$f(j_{x,0}, j_{y,0}) = \frac{1}{\epsilon_{w,x} \epsilon_{w,y}} \exp\left(-\frac{j_{x,0}}{\epsilon_{w,x}} - \frac{j_{y,0}}{\epsilon_{w,y}}\right). \quad (\text{S10})$$

The nonlinearity in the wakefield results in amplitude-dependent (i.e., action-dependent) betatron frequencies for the beam particles. Following canonical perturbation theory, an estimate for these frequencies (valid for  $\alpha_{[x,y]} \lesssim 1$ ) can be obtained by averaging over the angular coordinates the expressions for  $\theta_{[x,y]}/dz$  in Eq. (S9), namely

$$k_{\beta,[x,y]} = \frac{1}{(2\pi)^2} \int \int \left(\frac{d\theta_{[x,y]}}{dz}\right) d\theta_x d\theta_y. \quad (\text{S11})$$

For a flat beam,  $\epsilon_{w,x} \ll \epsilon_{w,y}$ , we have that, in general,  $j_{y,0} \ll j_{x,0}$ , and so the betatron frequencies are determined solely by the initial value of the particle's action in the horizontal plane. We obtain,

$$\begin{cases} \frac{k_{\beta,x}}{k_{\beta,0}} \simeq 1 + \alpha_x Q_2(j_{x,0}; L_x) \\ \frac{k_{\beta,y}}{k_{\beta,0}} \simeq 1 + \frac{\alpha_y}{2} Q_0(j_{x,0}; L_y) \end{cases} \quad (\text{S12})$$

where

$$Q_p(j_{x,0}; L) = \frac{1}{2\pi} \int_0^{2\pi} (\cos \varphi)^p H\left[\frac{2k_{\beta,0} j_{x,0} \cos \varphi}{(k_p L)^2}\right] d\varphi. \quad (\text{S13})$$

If the characteristic size of the nonlinearity is (much) larger than the characteristic size of the beam in the horizontal plane ( $\sigma_{w,x} \sim (\epsilon_{w,x}/\gamma_w k_{\beta,0})^{1/2} \ll L_{[x,y]}$ , we refer to this as the small beam limit), then  $k_{\beta,0} j_{x,0} \ll (k_p L_{[x,y]})^2$ , and so we can use the approximation  $H(q) \simeq 1 - q/2$ . In this limit the expressions for the betatron frequencies Eq. (S12) simplify to

$$\begin{cases} \frac{k_{\beta,x}}{k_{\beta,0}} \simeq 1 + \frac{\alpha_x}{2} \left[ 1 - \frac{3}{4} \frac{k_{\beta,0} j_{x,0}}{(k_p L_x)^2} \right] \\ \frac{k_{\beta,y}}{k_{\beta,0}} \simeq 1 + \frac{\alpha_y}{2} \left[ 1 - \frac{1}{2} \frac{k_{\beta,0} j_{x,0}}{(k_p L_y)^2} \right]. \end{cases} \quad (\text{S14})$$

Resonant particles are the ones for which the horizontal and vertical betatron frequencies lay within a narrow strip of size  $\sim \delta k_{\beta,0}$ , with  $\delta \ll 1$  (we will discuss later how to determine the size), around the  $k_{\beta,x} = k_{\beta,y}$  line in the plane of betatron frequencies.

Defining the quantity

$$R_p = \frac{1}{\epsilon_{w,x}} \int_0^\infty j_{x,0}^p \Theta\left(\delta - \left|\frac{k_{\beta,x}}{k_{\beta,0}} - \frac{k_{\beta,y}}{k_{\beta,0}}\right|\right) \times \exp\left(-\frac{j_{x,0}}{\epsilon_{w,x}}\right) dj_{x,0}, \quad (\text{S15})$$

where  $\Theta(q)$  is the Heaviside function, we have that the fraction of beam particles in the resonance is

$$\eta_r = R_0, \quad (\text{S16})$$



and the average value of the action for the resonant particles is

$$j_{x,0}^{(r)} = \frac{R_1}{R_0}. \quad (\text{S17})$$

Note that  $j_{x,0}^{(r)}$  is defined only when resonant particles are present (i.e., when  $\eta_r > 0$ ).

The expressions for  $\eta_r$  and  $j_{x,0}^{(r)}$  can be explicitly evaluated in the small beam limit. We obtain

$$j_{x,0}^{(r)} \simeq \frac{4k_p^2 L_x^2 L_y^2}{k_{\beta,0}} \frac{\alpha_x - \alpha_y}{3\alpha_x L_y^2 - 2\alpha_y L_x^2}. \quad (\text{S18})$$

Note that this expression is valid for values of  $\alpha_{[x,y]}$  and  $L_{[x,y]}$  such that the condition  $0 \leq k_{\beta,0} j_{x,0}^{(r)} \ll (k_p L_{[x,y]})^2$  is satisfied. Defining the auxiliary quantities

$$j_{\pm} = j_{x,0}^{(r)} \pm \frac{8k_p^2 L_x^2 L_y^2}{k_{\beta,0}} \frac{\delta}{|3\alpha_x L_y^2 - 2\alpha_y L_x^2|}, \quad (\text{S19})$$

(if  $j_- < 0$  we redefine it as  $j_- = 0$ ) we have

$$\eta_r \simeq \exp\left(-\frac{j_-}{\epsilon_{x,0}}\right) - \exp\left(-\frac{j_+}{\epsilon_{x,0}}\right). \quad (\text{S20})$$

The evolution of the angle coordinates for each beam particle can be obtained solving the first equation in Eq. (S9), neglecting oscillations on the  $\sim k_{\beta,0}^{-1}$  scale. We obtain

$$\theta_{[x,y]}(z) \simeq \theta_{[x,y],0} + k_{\beta,[x,y]} z, \quad (\text{S21})$$

where  $k_{\beta,[x,y]}$  are given by Eq. (S12).

The evolution of the actions is different for resonant and non-resonant particles. This can be seen rewriting the evolution equation for the action (second equation in Eq. (S9)) in the small beam limit, by using Eq. (S21) for the evolution of the angles, and by averaging over oscillations at the  $\sim k_{\beta,0}^{-1}$  scale. For non-resonant particles, i.e.,  $k_{\beta,x} \neq k_{\beta,y}$ , we have

$$\frac{dj_{[x,y]}}{dz} \simeq 0, \quad (\text{S22})$$

and so the actions in both planes are separately (quasi-)preserved during evolution, namely

$$j_{[x,y]} = j_{[x,y],0}. \quad (\text{S23})$$

For resonant particles, i.e.,  $k_{\beta,x} = k_{\beta,y}$ , we have

$$\begin{cases} \frac{dj_x}{dz} \simeq -k_{\beta,0}^2 \frac{\alpha_x}{4} \frac{j_x j_y}{(k_p L_x)^2} \sin 2(\theta_{x,0} - \theta_{y,0}) \\ \frac{dj_y}{dz} \simeq k_{\beta,0}^2 \frac{\alpha_y}{4} \frac{j_x j_y}{(k_p L_y)^2} \sin 2(\theta_{x,0} - \theta_{y,0}), \end{cases} \quad (\text{S24})$$

and so the actions in the two planes are not separately conserved since the nonlinearity provides a mechanism to couple the particle motion in the horizontal

and vertical planes. However, since  $(\alpha_y/L_y^2)(dj_x/dz) + (\alpha_x/L_x^2)(dj_y/dz) \simeq 0$ , we have that the quantity

$$\frac{\alpha_y}{L_y^2} j_x + \frac{\alpha_x}{L_x^2} j_y = \frac{\alpha_y}{L_y^2} j_{x,0} + \frac{\alpha_x}{L_x^2} j_{y,0} = \text{const.}, \quad (\text{S25})$$

is (quasi-)preserved, and the value of the constant is set by the initial condition for the actions. Using Eq. (S25) in Eq. (S24) we obtain the following equation describing the evolution of  $j_x$ ,

$$\begin{aligned} \frac{dj_x}{dz} &\simeq -\frac{k_{\beta,0}^2 \sin 2(\theta_{x,0} - \theta_{y,0})}{4} \\ &\times j_x \left[ \frac{\alpha_x}{(k_p L_x)^2} j_{y,0} + \frac{\alpha_y}{(k_p L_y)^2} (j_{x,0} - j_x) \right]. \end{aligned} \quad (\text{S26})$$

The asymptotic solution of this equation can be obtained as follows. If  $\sin 2(\theta_{x,0} - \theta_{y,0}) > 0$  (case I), then  $dj_x/dz < 0$  and so  $j_x$  decreases. The horizontal action will continue to decrease (the term within the square parenthesis is always positive) and will tend to the asymptotic value

$$j_x^{*,+} = 0, \quad (\text{S27})$$

which is a fixed point for Eq. (S26). At the same time Eq. (S25) implies that  $j_y$  will increase and tend to the asymptotic value

$$j_y^{*,+} = j_{y,0} + \frac{\alpha_y L_x^2}{\alpha_x L_y^2} j_{x,0} \simeq \frac{\alpha_y L_x^2}{\alpha_x L_y^2} j_{x,0}, \quad (\text{S28})$$

where the last equality is valid for a flat beam. Conversely, if  $\sin 2(\theta_{x,0} - \theta_{y,0}) < 0$  (case II), the opposite behaviour is observed: the horizontal emittance will tend to the asymptotic value

$$j_x^{*,-} = j_{x,0} + \frac{\alpha_x L_y^2}{\alpha_y L_x^2} j_{y,0} \simeq j_{x,0}, \quad (\text{S29})$$

while the vertical emittance approaches the asymptotic value

$$j_y^{*,-} = 0. \quad (\text{S30})$$

Note that since  $\theta_{x,0} - \theta_{y,0}$  is uniformly distributed in  $[0, 2\pi]$ , the solutions corresponding to case I and case II occur with the same probability. We discussed the exchange of the actions for the case  $k_{\beta,x} = k_{\beta,y}$  (i.e., a perfect resonance). However, a similar behavior is observed if the difference between the betatron frequencies in the two planes is less than the characteristic width of the resonance. This width, which depends on the strength of the coupling between the horizontal and vertical degrees of freedom, can be determined numerically, and for the parameters considered in this work we can assume

$$\delta \approx 0.02(\alpha_x \alpha_y)^{1/2}, \quad (\text{S31})$$

valid if  $L_x \simeq L_y$ . Even though these results have been derived in the small beam limit, a direct numerical solution of Eq. (S9) demonstrates that the results continue

to hold, at least approximately, as long as the beam is not too large.

We can now compute the beam emittance at saturation when mixing occurs. We recall that the beam emittance in each plane is given by the average value of the action in that plane if the angle coordinates are uniformly distributed. By separating the contribution of resonant and non resonant particles we have

$$\epsilon_{w,[x,y]}^* \simeq (1 - \eta_r) \langle j_{[x,y]}^* \rangle_{\text{non-res.}} + \eta_r \langle j_{[x,y]}^* \rangle_{\text{res.}}, \quad (\text{S32})$$

where  $\langle j_{[x,y]}^* \rangle_{\text{non-res.}}$  and  $\langle j_{[x,y]}^* \rangle_{\text{res.}}$  are the average values of the action at saturation for non-resonant and resonant particles, respectively. Considering that, in general,  $\eta_r \ll 1$ , then from Eq. (S23) and Eq. (S10) we obtain

$$\langle j_{[x,y]}^* \rangle_{\text{non-res.}} \simeq \epsilon_{w,[x,y]}. \quad (\text{S33})$$

For resonant particles, using Eqs. (S27), (S28), (S29), (S30), and considering that the initial value of the action for such resonant particles is given by Eq. (S17), we have

$$\begin{cases} \langle j_x^* \rangle_{\text{res.}} = \frac{1}{2} j_x^{*,+} + \frac{1}{2} j_x^{*,-} \simeq \frac{1}{2} j_{x,0}^{(r)} \\ \langle j_y^* \rangle_{\text{res.}} = \frac{1}{2} j_y^{*,+} + \frac{1}{2} j_y^{*,-} \simeq \frac{1}{2} \frac{\alpha_y}{\alpha_x} \frac{L_x^2}{L_y^2} j_{x,0}^{(r)}. \end{cases} \quad (\text{S34})$$

By inserting Eqs. (S33) and (S34) into Eq. (S32), we obtain the following expression for the emittances at saturation

$$\begin{cases} \epsilon_{w,x}^* \simeq (1 - \eta_r) \epsilon_{w,x} + \frac{1}{2} \eta_r j_{x,0}^{(r)} \\ \epsilon_{w,y}^* \simeq (1 - \eta_r) \epsilon_{w,y} + \frac{1}{2} \eta_r \frac{\alpha_y}{\alpha_x} \frac{L_x^2}{L_y^2} j_{x,0}^{(r)} \end{cases} \quad (\text{S35})$$

We see that, whenever resonant particles are present (i.e.  $\eta_r > 0$ ), mixing occurs: the horizontal beam emittance decreases, while the vertical one increases. Figure 2 (d) in the Letter shows the growth of the geometric average of the emittances after mixing,  $(\epsilon_{w,x}^* \epsilon_{w,y}^* / \epsilon_{w,x} \epsilon_{w,y})^{1/2}$ , as a function of the angle  $\arctan(\alpha_y / \alpha_x) / \pi$ , obtained using Eq. (S35) (and using the values of  $\eta_r$  and  $j_{x,0}^{(r)}$  from Eqs. (S16), (S17), respectively). The beam and wake parameters are the ones discussed in the Letter. The theoretical prediction is in good agreement with the test particle simulation results.

In the small beam limit, the expression for the emittances at saturation can be obtained by using Eqs. (S18) and (S20) in Eq. (S35).